Available online at www.sciencedirect.com
SCIENCE DIRECT®
Biomaterials 26 (2005) 7650–7660
Biomaterials
www.elsevier.com/locate/biomaterials

A transmission electron microscopy study of mineralization in age-induced transparent dentin

Alexandra E. Porter[a], Ravi K. Nalla[b,c], Andrew Minor[a], Joerg R. Jinschek[a], Christian Kisielowski[a], Velimir Radmilovic[a], John H. Kinney[d,e], Antoni P. Tomsia[b,c], R.O. Ritchie[b,c,*]

[a]*Lawrence Berkeley National Laboratory, National Center for Electron Microscopy, Berkeley CA 94720, USA*
[b]*Materials Sciences Division, Lawrence Berkeley National Laboratory, University of California, Berkeley CA 94720-1760, USA*
[c]*Department of Materials Science and Engineering, 381 Hearst Mining Building, MC 1760, University of California, Berkeley, CA 94720-1760, USA*
[d]*Department of Mechanical Engineering, Livermore, CA 94550,USA*
[e]*UCSF/UCB Joint Graduate Group in Bioengineering, Lawrence Livermore National Laboratory, Livermore, CA 94550, USA*

Received 8 March 2005; accepted 17 May 2005
Available online 11 July 2005

Abstract

It is known that fractures are more likely to occur in altered teeth, particularly following restoration or endodontic repair; consequently, it is important to understand the structure of altered forms of dentin, the most abundant tissue in the human tooth, in order to better define the increased propensity for such fractures. Transparent (or sclerotic) dentin, wherein the dentinal tubules become occluded with mineral as a natural progressive consequence of aging, is one such altered form. In the present study, high-resolution transmission electron microscopy is used to investigate the effect of aging on the mineral phase of dentin. Such studies revealed that the intertubular mineral crystallites were smaller in transparent dentin, and that the intratubular mineral (larger crystals deposited within the tubules) was chemically similar to the surrounding intertubular mineral. Exit-wave reconstructed lattice-plane images suggested that the intratubular mineral had nanometer-size grains. These observations support a ''dissolution and reprecipitation'' mechanism for the formation of transparent dentin.

Keywords: Dentin; Transmission electron microscopy; Mineralization; Sclerotic; Transparent; Aging

1. Introduction

Dentin, the most abundant mineralized tissue in the human tooth, is composed largely of type-I collagen fibrils and nanocrystalline apatite mineral [1]. The most striking microstructural feature in normal, healthy dentin is the dentinal tubule—cylindrical channels, which are roughly 1–2 μm in diameter and course continuously from the dentin-enamel and the cementum-enamel junctions to the pulp with a thin, highly mineralized cuff of peritubular dentin surrounding each tubule. With aging, however, normal dentin is altered to form what is known as ''transparent'' (or sclerotic) dentin (Fig. 1). The tubules gradually fill up with a mineral phase over time, beginning at the apical end of the root and often extending into the coronal dentin [2,3], possibly due to a passive chemical precipitation process [4,5], decreasing the amount of light scattered off of the lumens. Physiologic transparent (or sclerotic) dentin, as distinguished from pathologic transparency often seen subjacent to caries, appears to form without trauma or caries attack as a natural consequence of aging [2].

*Corresponding author. Department of Materials Science and Engineering, 381 Hearst Mining Building, MC 1760, University of California, Berkeley, CA 94720-1760, USA. Tel.: +1 510 486 5798; fax: +1 510 486 4881.
E-mail address: roritchie@lbl.gov (R.O. Ritchie).

0142-9612/$ - see front matter © 2005 Elsevier Ltd. All rights reserved.
doi:10.1016/j.biomaterials.2005.05.059

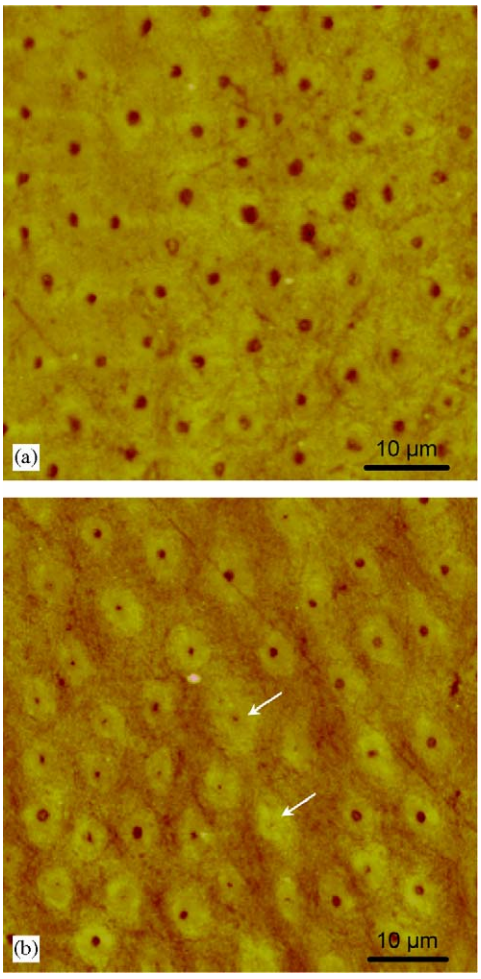

Fig. 1. Atomic force microscopic images of (a) normal (donor age = 25 years) and (b) transparent (donor age = 67 years) dentin. The dark contrast indicates the tubule sites and the white arrows in (b) show representative tubule lumens occluded with mineral (courtesy: M. Balooch).

Dentin transparency thus is a commonly observed pathology in aged teeth, but it is unclear if the increased mineralization is from the filling of the tubule lumens [2], or whether there are any additional alterations in the mineralization of the intertubular dentin matrix [6,7]. Our previous work using small-angle X-ray scattering (SAXS) revealed a slightly lower mineral crystallite size in transparent dentin, as compared to normal dentin [8]. However, it was recognized that differences in the scattering from the filled tubules lumens might affect such results, and hence, more direct measurements are necessary to evaluate the nanostructural changes in the mineralization associated with age-induced transparency.

While transmission electron microscopy (TEM) has been used for examining dentin at such size scales, with a number of such investigations being reported in archival literature over the last 60 years (e.g. [9–26]), most of these studies have been restricted to healthy, non-transparent dentin. Indeed, to the authors' knowledge, there have been only a handful of studies that have sought to investigate altered forms of human dentin, particularly for dentinogenesis imperfecta (e.g. [13,15]) and caries-affected/carious dentin (e.g. [14,27]). In carious dentin, tubule filling is also seen, akin to that in transparent dentin, although this is induced by bacterial action, with a mechanism involving dissolution of surrounding apatite intertubular mineral and its reprecipitation within the tubules as magnesium-rich beta-tricalcium phosphate (β-TCP/ whitlockite) and apatite [27]. In the present work, we seek to address this paucity of data on transparent dentin through a TEM-based study of the mineral phase in dentin; specifically, we examine the crystallite size and chemical nature of the mineral associated with intertubular dentin in age-induced transparent dentin in comparison to normal (non-transparent) dentin. We also examine the mineral accreted within the tubule lumens in transparent dentin. The null hypotheses being tested here are: (1) the intertubular mineral crystallite size decreases with transparency and (2) the mineral deposited in the tubules is chemically different from the intertubular mineral. This study is aimed at furthering our micro-mechanistic understanding of age-related changes in dentin biomineralization.

2. Materials and methods

2.1. Materials

Recently extracted transparent ($N = 8$, donor age (mean $\pm$ S.D.): 80.2 $\pm$ 9.5 years) and normal ($N = 5$, donor age (mean $\pm$ S.D.): 23.5 $\pm$ 0.6 years) human molars, obtained from a total of 13 donors, according to protocols approved by the University of California San Francisco Committee on Human Research, were used; each tooth was sterilized using gamma radiation after extraction [28]. Sections (~1.5–2.0 mm thick) were prepared vertically through the teeth (see Fig. 2a), from which beams measuring ~0.9 × 0.9 × 10.0 mm were machined, with one beam being obtained per tooth (Fig. 2b). Samples were then obtained from these sections by wet polishing up to a 600 grit finish, and stored in Hanks' balanced salt solution at ambient temperature for no longer than 1 week until actual specimen preparation.

2.2. Specimen preparation

Sections were prepared using both ultramicrotomy and focused ion-beam milling (as a secondary technique for transparent dentin). By using two different sample preparation methods, any artefacts resulting from the process of thinning the samples to electron transparency could be monitored.

2.2.1. Ultramicrotomy

The beams ($N = 5$ each for transparent and normal dentin) were treated with three changes of 100% ethanol over 15 min

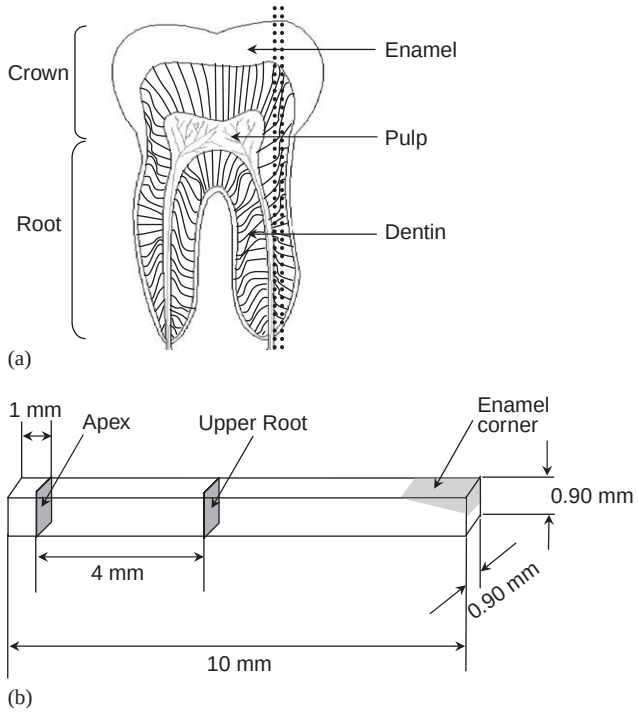

Fig. 2. Schematic illustration of (a) a typical human tooth with the section (shown by dotted line) made for the purpose of specimen preparation and (b) the dentin beam with the location of the TEM specimens being indicated.

to dehydrate them and three changes of acetonitrile (a transitional solvent) over 1 h. The beams were then infiltrated with Spurr's resin (Agar Scientific, Essex, UK) over the period of several days. Spurr's resin was prepared with 10 g epoxy monomer vinyl cyclohexene dioxide (ERL), 4.5 g diglycidyl ether of polypropylene glycol (DER-736), 26 g nonenyl succinic anhydride (NSA), and 0.7 g benzyldimethylamine (BDMA). The samples were agitated at room temperature in 1:1 solutions of acetonitrile and Spurr's resin for 1 day, in a 1:3 acetonitrile, specifically, Spurr's solution for 1 day (both steps performed in ambient air) and then in 100% Spurr's for 2 weeks in vacuo. In each case, the Spurr's resin was changed every 24 h. Samples were then cured in fresh Spurr's resin for 24 h at 60 °C. Pre-casting a ~200 μm layer of Spurr's resin into the truncated beam capsules before adding the teeth facilitated initial sectioning of the blocks. Fifty to seventy nanometer thick sections were then cut onto distilled water with an ultramicrotome (Boeckeler Instruments Inc., Tuscon, AZ) using a 35° diamond knife. Sections were collected immediately on lacey carbon 300 mesh copper grids, and dried for 1 h at 37°C [29]. Such sections were obtained from two particular areas of interest: (1) near the tooth apex and (2) the upper root region (Fig. 1b), with at least three sections per area of interest being prepared. Sections were cut both parallel and perpendicular to the long axis of the beams.

2.2.2. Focused ion beam milling

Sections, ~1 × 1 × 1 mm, were carefully cut with a regular slow-speed (~100 RPM) diamond saw (TechCut II, Allied High Tech Products Inc., Rancho Dominguez, CA) from the apex region in the beams of transparent dentin ($N = 3$). Each section was then mounted using AE15 (M-bond) adhesive kit on a 2 × 1 mm copper slot grids grid (SPI Supplies, West Chester, PA). Following this step, the samples were pre-thinned to about 50–60 μm using a conventional grinder (Minimet 1000, Buehler Inc., Lake Bluff, IL) and dimpler (VCR Dimpler 296 D500i, South Bay Technology Inc., San Clemente, CA) and then carbon coated to minimize specimen charging during the ion-beam milling.

The area of interest (filled tubules in transparent dentin) in each coated sample were then reduced to a thickness of ~100 nm to ensure sufficient electron transparency for transmission electron microscopy. This was achieved using a dual-beam focused ion-beam (FIB) system (Strata 235, FEI Company, Hillsboro, OR), which contained both a focused gallium ion beam and a conventional field-emission scanning electron column. The ion beam was operated at 30 kV with varying beam current ranging from 20 nA to 100 pA as the electron-transparent portion of the sample became thinner.

2.3. Transmission electron microsopy

TEM studies were performed on a JEOL 3010 (JEOL USA Inc., Peabody, MA), FEI-Philips CM200 and FEI-Philips CM300 FEG-TEMs (FEI Company, Hillsboro, OR). Low-magnification, bright-field imaging, selected-area electron diffraction (SAED) and microdiffraction were performed on the JEOL 3010; high-resolution lattice imaging was performed on the CM300.

2.3.1. Crystal size (width) determination

In order to determine if there is a change in the intertubular mineral crystallite size with transparency, TEM micrographs obtained at magnifications of 100,000 times were used. The plate width (short axis of the needle-like crystals) was measured for crystals that could be clearly distinguished in these micrographs; at least 70 such crystals were examined for each case (dentin type and location). Means and standard deviations for these data were calculated; statistical differences were examined using a two-tail unpaired t-test (Welch corrected) and the corresponding P values reported ($P < 0.05$ was considered statistically significant, $0.05 < P < 0.10$ weakly significant, and $P > 0.10$ not significant).

2.3.2. Crystal structure determination

SAED patterns were taken for the intertubular dentin from the apex and upper root regions of the teeth in five different areas in both the normal and transparent dentin sections, and also for the intratubular mineral in the case of transparent dentin. The SAED patterns were indexed by calculating ratios between the major rings and comparing these to simulated diffraction patterns for the hydroxyapitite (HA) structure (MacTempas, Total Resolution, Berkeley, CA).

2.3.3. Exit-Wave (EW) reconstuction

The complex contrast transfer function of field-emission electron microscopes results in high-resolution TEM lattice images, which are complex beam interferrograms and are not straight-forward to interpret [30]. In contrast, object exit-plane phase images can provide direct images of the crystal structure

with minimal distortions of thin samples (thickness $t <$ extinction distance). Processing of a focal series of lattice images allows recovering of the complex electron object EW function. In the holographic reconstruction process, the defocus dependence of lattice image patterns is eliminated and delocalization as well as lens aberrations up to the third order can largely be reduced [31]. Further, the procedure pushes the directly interpretable resolution down to the information limit of the microscope.

In order to further examine the crystals, EW reconstructions were performed on Berkeley's One Ångström Microscope (OAM), a Philips CM300 FEG/UT-TEM (spherical aberration coefficient, $C_s = 0.6$ mm) [32,33]. Focal series were taken in 20 different areas from the intertubular dentin in transparent dentin and normal dentin, and from the intratubular dentin in transparent dentin. Twenty images were used for each focal series, with a starting focus of −260 nm and a focal increment of 2 nm. The total exposure time of the focal series was 2 min. Reconstructions were performed using the "TrueImage" program package (FEI Company, Hillsboro, OR) that is based on the PAM/MAL (Paraboloid/ Maximum-Likelihood) algorithm by Thust et al. [30], and Coene et al. [34]. The reconstructed images were examined to determine the crystallographic structure of the crystals inside the tubules.

2.3.4. Beam damage experiments

TEM beam–specimen interactions have previously been reported to induce some damage to the mineral phase in human dental enamel [35]. In order to confirm that neither a phase transformation nor crystal growth had arisen from electron-induced damage during the imaging process, short time-elapsed "films" were taken of the dentin at the edge of the tubules in a section of the transparent dentin. Images were captured after 2 s, 1 min and 2 min of exposure (i.e., the exposure time of the focus series used previously for the EW reconstructions). These images and the corresponding fast Fourier transforms (FFTs) were examined for time-dependent changes to the mineral phase.

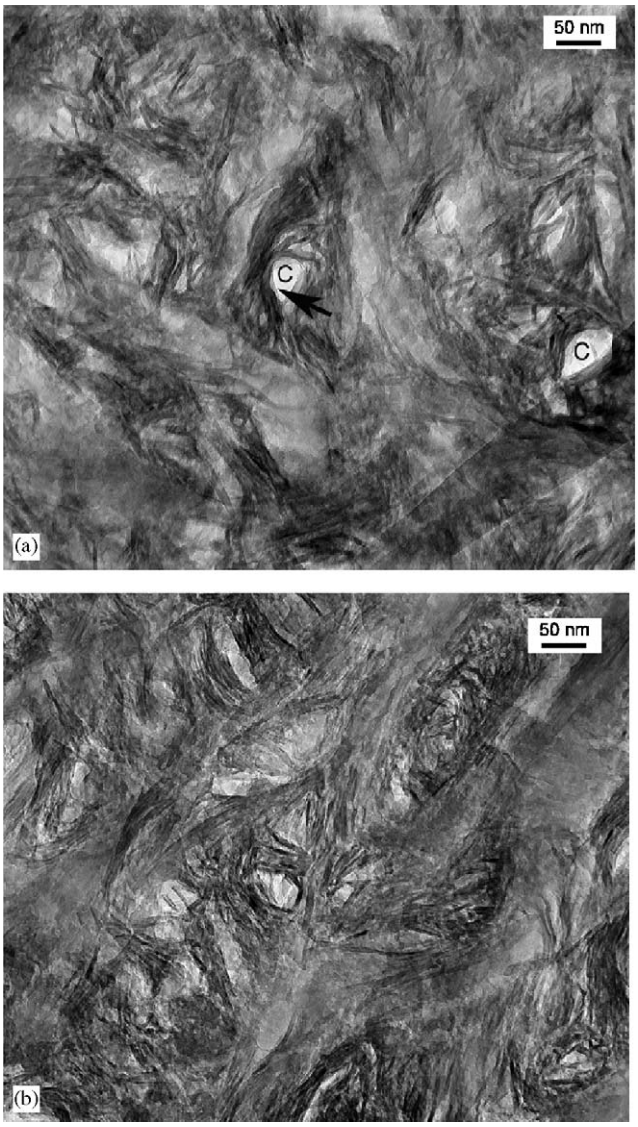

Fig. 3. TEM micrographs of the intertubular mineral in (a) transparent and (b) normal dentin taken from the apex region. The black arrow in (a) indicates the "bending" of crystals around voids (marked "C").

3. Results

3.1. Intertubular dentin crystallites

Transparent and normal dentin intertubular mineral crystallites appeared needle-like in morphology when observed on edge, similar to previous observations by others in dentin and bone, e.g., [14,36]. Figs. 3a and b show typical TEM micrographs for dentin from the apex region. There were no observable qualitative differences in the morphology between dentin types or across regions. Although the crystallites were predominantly straight and needle-like, in some instances, and particularly around voids, crystallites bent around the circumference of the voids were observed (Fig. 3a). High-resolution lattice imaging of the intertubular dentin revealed individual plate-like apatite crystallites (Fig. 4).

The crystallite width was determined from the TEM images at both locations for both dentin forms. At both the apex and upper root regions, qualitative and quantitative observations indicated a decrease in the crystallite width with dentin transparency, with a decrease of 7–19% in the mean crystallite width (Table 1). Unpaired t-tests revealed that such differences across dentin types were very significant for the upper root region ($P < 0.0001$) and weakly significant for the apex region ($P = 0.0845$). There were no significant differences with location in the transparent dentin ($P = 0.6355$), but such differences were significant in normal dentin ($P = 0.0004$). These differences and the crystallite widths measured are generally consistent with our prior SAXS findings [8]. This provides conclusive

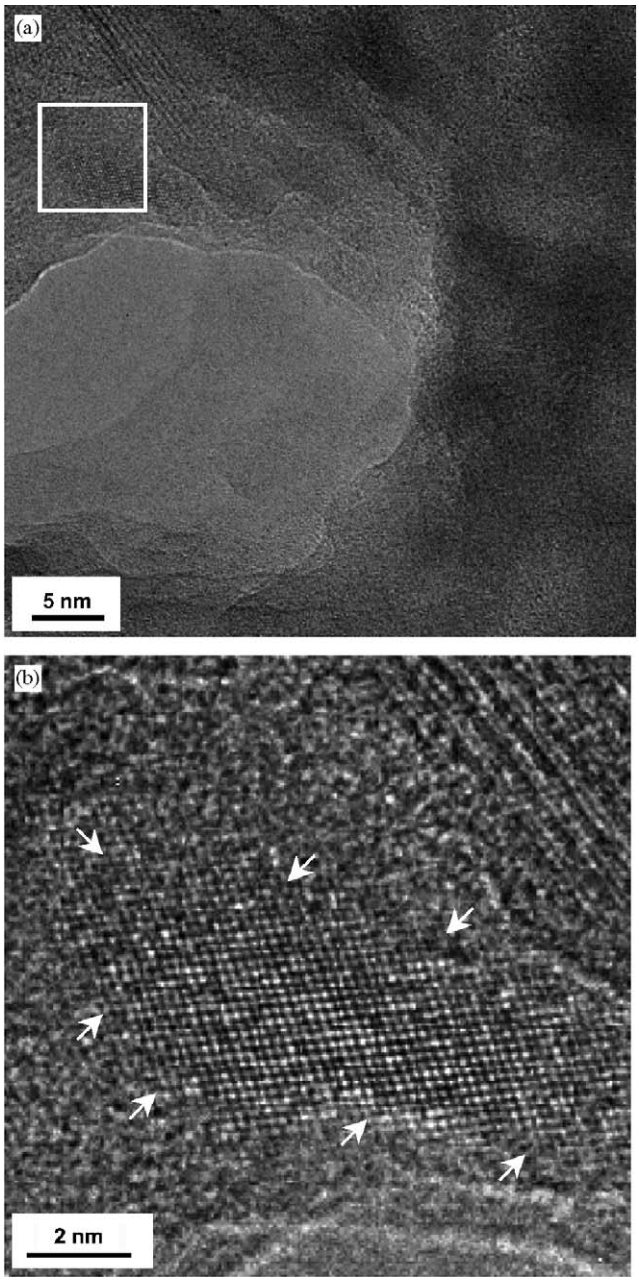

Fig. 4. (a) Low- and (b) high-magnification lattice images of the intertubular mineral in transparent dentin. The enclosed region in (a) in magnified in (b). The regular, periodic arrangement of the lattice fringes indicates that each mineral crystallite (shown by white arrows in (b)) is oriented in a single direction. Note another crystal in a different orientation at the top, right corner of (b).

evidence that the crystallites are slightly wider in the normal dentin as compared to the transparent dentin, confirming the first hypothesis proposed here. Furthermore, location-dependent differences in crystallite width appear to be reduced with transparency.

SAED patterns obtained for both regions were analogous in all the areas investigated in both transparent and normal dentin. A representative SAED pattern is illustrated in Fig. 5 for transparent dentin from the apex location. Indexing of the principal rings in this pattern, i.e., the (0 0 2) and (300/112 and 211) rings, confirmed that the peritubular crystallites belonged to the hydroxyapatite phase.

3.2. Intratubular crystallities in transparent dentin

Dentinal tubules ~1 μm in diameter, partially filled with mineral crystals, were clearly identifiable, when sections with areas perpendicular to the long axis of the tubules were examined (Figs. 6a and b). The mineral within the tubule lumens appeared to be substantially coarser (~100 nm plate width) and had darker contrast than that in the intertubular dentin (~4–6 nm plate width).

In many regions, similar features were observed in transparent dentin samples prepared by FIB milling; plate-like apatite crystallites were present within the intertubular dentin and coarser crystals were found within the tubules. In FIB-ed sections, the intratubular crystallites were more clearly shown to emanate from the intratubular dentin at the tubule edge (Fig. 6c). The tubules appeared to be more filled up in the FIB-ed case, as some of the occluded mineral might have been lost during preparation using ultramicrotoming, which in this case might not have left the filled-tubule structure entirely intact.

Indexing of the SAED patterns from the intratubular crystals (Fig. 7) showed it was hydroxyapatite, akin to the intertubular mineral (Fig. 5). Note that the individual spots are more clearly delineated for the intratubular mineral, as compared to those obtained for the intertubular case (Fig. 5), supporting the larger intratubular crystal size.

3.3. EW reconstructions

To gain possible mechanistic insight into these age-induced changes in the mineralization, high-resolution

Table 1
Mineral crystallite sizes in transparent and normal dentin[a]

Dentin type	Specimen location	Mean Size (nm)	S.D. (nm)	No. of crystallites measured
Transparent	Apex	4.52	0.77	73
Transparent	Upper root	4.47	0.77	97
Normal	Apex	4.84	1.36	73
Normal	Upper root	5.54	1.07	94

[a]Differences between individual donors in a group were not significant at both locations.

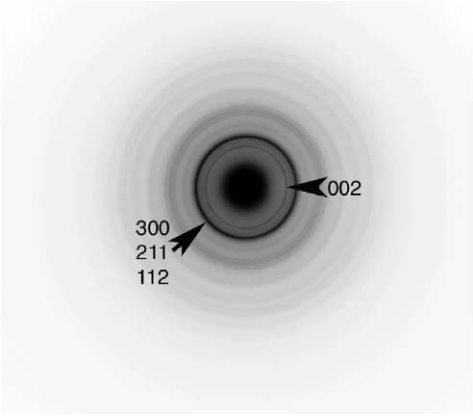

Fig. 5. SAED pattern for intertubular mineral in transparent dentin, with the indexing confirming the presence of hydroxyapatite.

TEM was performed on the intratubular mineral. Only crystallites located at the edge of the tubules were thin enough (<10 nm) to perform these experiments. EW reconstructions of each focus series enabled differentiation of atomic columns within the large crystals (Fig. 8). Fig. 8a clearly shows that the crystals comprised well-defined single crystal grains sharing a common direction. Evidence of faceting was also seen. Diffractograms of selected areas within the reconstructions (Fig. 8b) showed that, in addition to the hydroxyapatite previously identified, some of the domains were face-centered cubic (fcc) and the atomic spacing matched that of CaO ($d_{100} = 4.8$ Å).

In order to confirm that the nanocrystalline structure of the intratubular mineral was real and not formed as a result of electron-induced damage, 3 min long films of the dentin at the edge of the tubules were taken (i.e., 1 min longer than the total exposure time of the focus series), and still images captured at 1, 60 and 120 s (Fig. 9a–c). Fourier transforms of selected areas showed that the crystals rotated after exposure to the electron beam (Fig. 9b). No evidence of crystal growth or phase transformation was found over the time period we investigated.

4. Discussion

Transparency in a common age-induced pathology in human dentin and has been associated with a definitive reduction in the fracture resistance [8]. An understanding of the corresponding changes to the underlying ultrastructure is important from the perspective of evaluating age-related changes in the mineralization and could assist in the design of measures to counter its deleterious effects. In the present study, we have used high-resolution TEM techniques combined with electron diffraction and microanalysis to examine how such ultrastructure in dentin changes with age. However, as

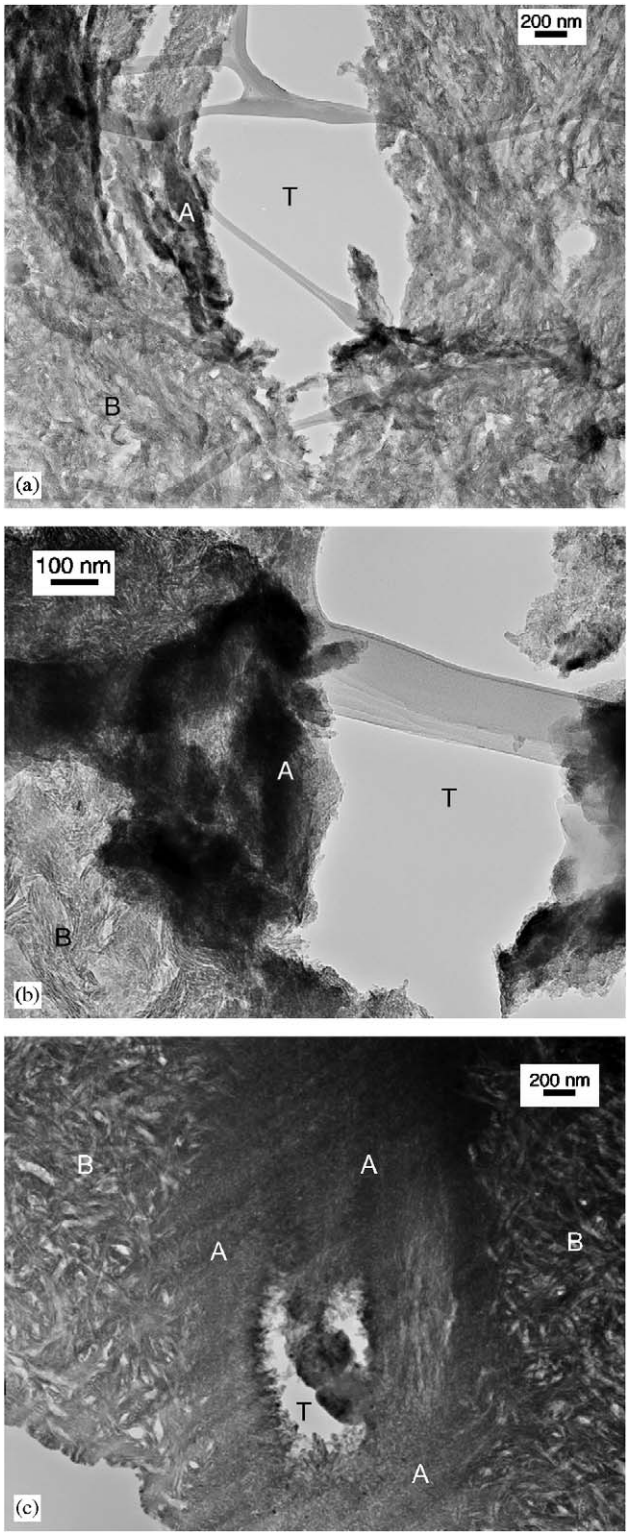

Fig. 6. TEM micrographs obtained for specimens taken from around partially occluded tubules in transparent dentin. (a) and (b) are low- and high-magnification images, respectively, obtained from microtomed specimens, while (c) is from a FIB-ed sample. Note the much larger crystallite size of the intratubular mineral. T = tubule, A = intratubular mineral, B = intertubular mineral.

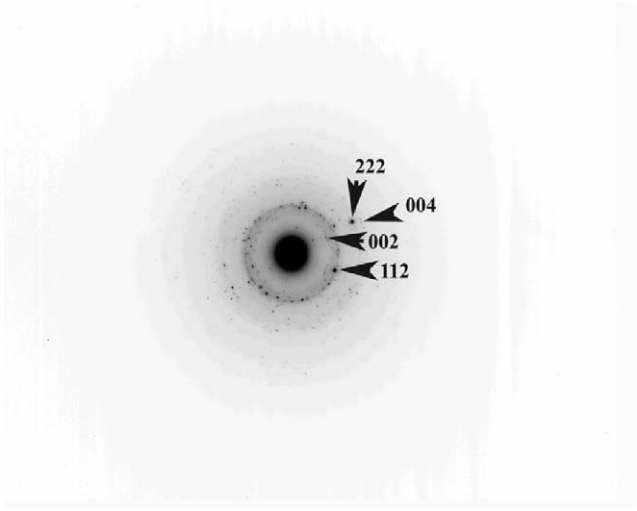

Fig. 7. SAED patterns obtained for the intratubular mineral in transparent dentin; the indexing confirmed the presence of hydroxyapatite. Note that the spots are more clearly delineated in this pattern, as compared to those obtained for the intertubular mineral (Fig. 5), supporting the larger intratubular crystal size.

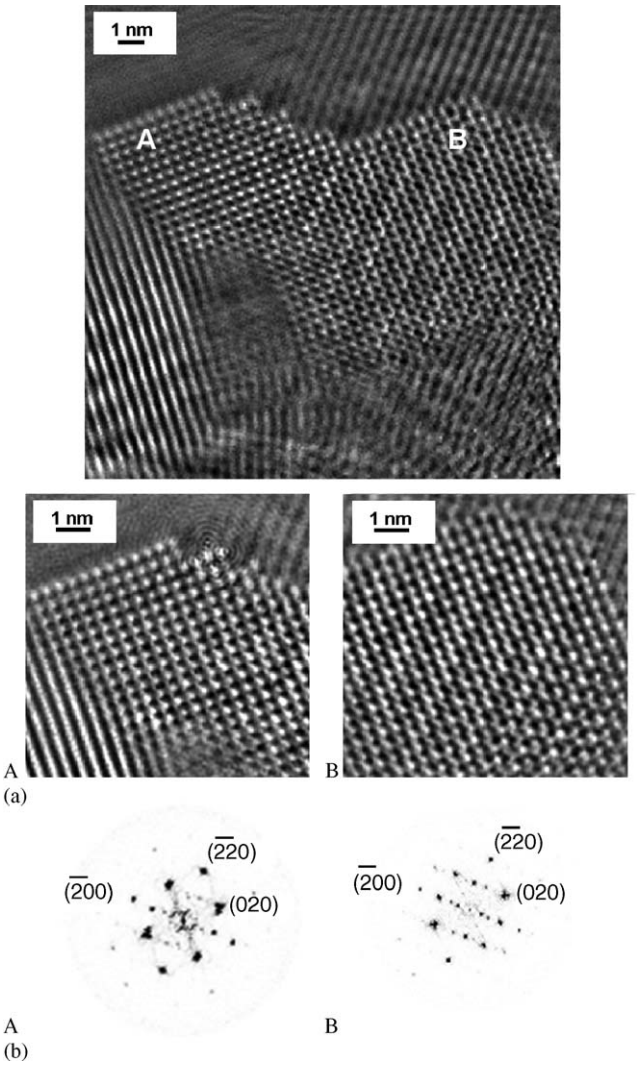

Fig. 8. (a) Reconstructed EW phase images obtained for the intratubular crystals showing evidence of nanometer-sized single crystal grains within; A shows an individual nanocrystal, while B shows a Moire pattern due to overlapping of two such nanocrystals. (b) FFTs showing the fcc structure in [0 0 1] zone axis orientation for the areas shown in A and B above. Note in B the presence of additional spots due to the overlapping of the nano-sized grains.

with any TEM study of biological tissues, there is always a concern that specimen preparation and exposure to the electron beam may damage the samples, thereby inducing artificial results. As detailed in Appendix A.1, we reason that the sample preparation techniques and exposure times used in the present work did not cause any such artifacts.

Indeed, we believe that this work has convincingly demonstrated changes in mineral size in dentin with age. Specifically, we find that there is a decrease in crystal width in intertubular dentin and that the dentinal tubules become occluded by larger crystals. These observations provide valuable insights into the possible mechanisms involved in tubule occlusion with age-induced transparency.

There has been some debate as to the chemical and crystallographic nature of the intratubular mineral in dentin. In carious dentin, electron diffraction experiments have shown that the intertubular phase is a combination of Mg-substituted β-TCP and apatite [27]. Our current SAED experiments show that the majority of the intratubular mineral in transparent dentin is hydroxyapatite; there was no evidence of Mg-rich β-TCP in the tubule lumens. Surprisingly, some nano-sized single-crystal grains found on the edge of the intratubular dentin were characterized to have an fcc structure and the interplanar spacing corresponded with that of CaO. From our current understanding, it is difficult to explain why CaO would form as a result of a physiochemical phenomena. Brès et al. [35] also observed an fcc phase and suggested it arises from an electron-beam-induced phase transformation. Although our beam damage experiments appear to rule out this possibility, the sample is momentarily exposed to the beam and an fcc phase may form. Future work is needed to address the nature and origin of the fcc phase, and is currently being undertaken.

Quantitative TEM observations made in the current study illustrate that the intertubular mineral crystallite size decreased significantly with age (Table 1). These findings confirm the validity of our previous SAXS results, which also revealed a slightly lower mineral crystallite size in transparent dentin, as compared to normal dentin [8]. Furthermore, within the tubules, the mineralization pattern was different in that with age, they became partially filled by larger crystals. A smaller mean intertubular crystal size could be the result of

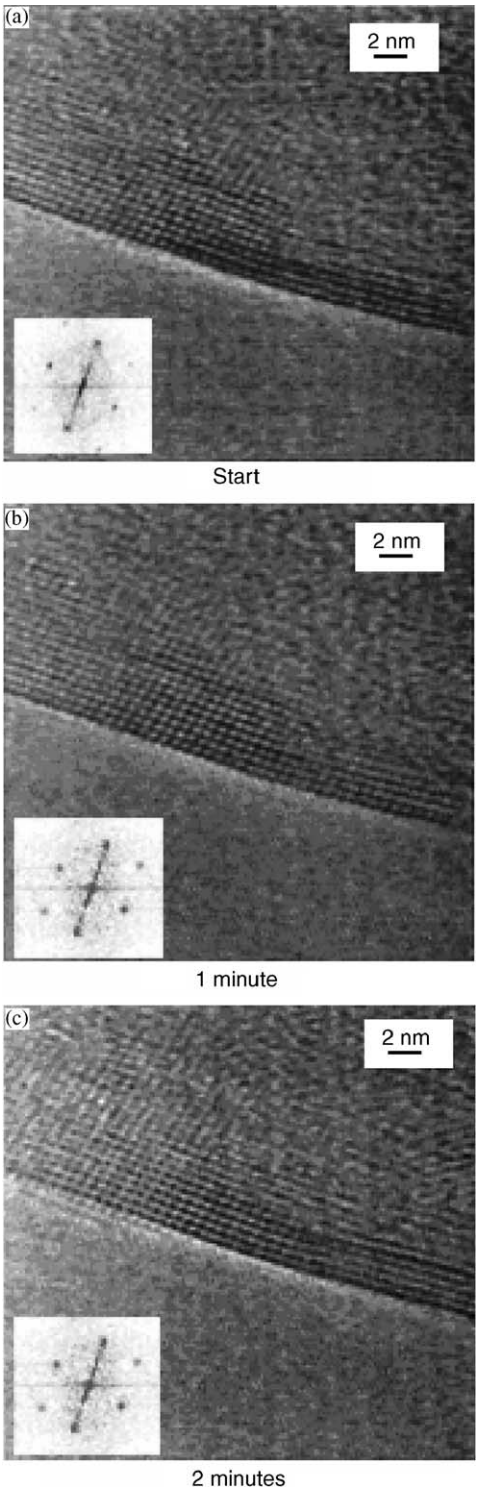

Fig. 9. A time-sequence of TEM images (corresponding diffraction patterns as insets) obtained during the beam damage experiments on the intratubular mineral in transparent dentin. No evidence of crystal growth or phase transformation was found with exposure to the electron beam.

dissolution of mineral from the intertubular matrix, which is then deposited into the tubules. The similar chemical composition of the inter- and intra tubular mineral in transparent dentin supports such a "dissolution-reprecipitation"-type mechanism; a similar mechanism has previously been proposed for carious dentin [27]. On the other hand, it is also possible that the dissolved mineral is re-deposited within the intertubular matrix instead of within the tubule lumens. We did not observe any new, smaller crystallites that such a mechanism would entail, and hence any mineral accretion within intertubular dentin can be ruled out. Consequently, we suggest that with age, the intertubular crystals dissolve uniformly, thereby decreasing in size, and that the mineral is reprecipitated within the tubules as a result of an increased saturation of calcium and phosphate ions within the dentin tubules.

High-resolution imaging in this study revealed a significant difference in the structure of the inter- and intra tubular dentin; notably polycrystalline grains were observed within the intratubular dentin crystals (Fig. 8). In comparison, within the intertubular dentin, individual plate-like apatite crystallites were found, with the entire crystallite being oriented in one single direction and surrounded by an amorphous matrix. This difference in nanostructure suggests a difference in the mechanism of mineral formation and in particular, that the intratubular dentin is formed by heterogeneously nucleated precipitation of the hydroxyapatite phase. These findings support our previous suggestion of a "dissolution-reprecipitation" mechanism as the etiology of dentin transparency.

With respect to the effect of these biological changes, based on our previous work, we note that the filling up of the tubules in transparent dentin has important consequences on the mechanical properties of dentin [8]. The tubules are believed to be the sites of microcrack nucleation [37], and hence play a critical role in the formation of the so-called "uncracked ligaments"[1] that form along the crack length; these intact regions, often tens of micrometers in size, act as bridges of material across the crack faces that hold cracks together, increasing the fracture resistance of the material [8,38,39]. In transparent dentin, there is consequently very little bridging, and the measured fracture toughness has been found to be lower by ~20% compared to normal dentin (~1.46 vs. ~1.79 $MPa\sqrt{m}$ [8]). This decreased fracture resistance has a clinically significant impact as it reduces the critical flaw size required for failure. Given that dentin is the most abundant tissue in the human tooth, with a consequent important role in the mechanical integrity of the tooth, age-induced transparency would be a contributing factor to the increased fragility of teeth often observed in older individuals.

[1]In the context of fracture, "ligament" here refers to any unfailed material, i.e., a crack "bridge", of any type, shape, and size, that spans the crack; not a ligament in the anatomical sense.

Finally, this work has provided evidence supporting a "dissolution-reprecipitation" mechanism for the formation of age-induced transparent dentin. We believe that this study offers an interesting case study of how aging produces simple microstructural alterations (without the complications introduced by extensive remodelling as in the case of bone), with consequences for the properties of the tissue. It is not yet clear what the biological and physico-chemical reactions underlying such alterations are. It is also important to examine the role of specific chemical species on such a mechanism. For example, fluoride ions are known to reduce the dissolution of apatites [40] and in low doses, reduce the risk of dental caries [41], thought the mechanisms involved again are not well understood. It is conceivable that the reduced dissolution may have beneficial effects with regards to the process of dentin transparency. In vitro experiments in a simulated body fluid have previously been used to shed light on dissolution–reprecipitation reactions in synthetic apatites [42]. Similar studies are currently being planned.

5. Conclusions

Based on a TEM-based study of the effect of aging on the mineral phase in dentin, the following conclusions can be drawn:

1. The intertubular mineral crystallites were some 7–19% smaller in age-induced (donor age : $\geqslant$65 years) transparent dentin as compared to normal dentin from normal donors (donor age: 25–35 years), and were chemically similar.
2. The large intratubular mineral crystals deposited within the tubules in transparent dentin were chemically similar to the intertubular mineral. High-resolution EW reconstructed lattice-plane images suggested that these large crystals were actually composed of nanometer-size grains.
3. These observations support a "dissolution and reprecipitation" mechanism for the formation of transparent dentin.

Acknowledgements

This work was supported by the National Institutes of Health under Grant Nos. 5R01 DE015633 and P01DE09859 (for R.K.N., J.H.K., A.P.T., R.O.R.), and by the Director, Office of Science, Office of Basic Energy Science, Division of Materials Sciences and Engineering, Department of Energy under No. DE-AC03-76SF00098 (for A.E.P., A.M., J.R.J., C.F.K., V.R.). The authors acknowledge the use of the facilities of the National Center for Electron Microscopy at the Lawrence Berkeley National Laboratory, also funded by the Department of Energy. They also wish to thank Profs. S.J. and G.W. Marshall, (University of California, San Francisco) and Dr. M. Balooch for many useful discussions, and Ms. G. Nonomura for help with the dentin beam preparation.

Appendix A. Potential damage from TEM sample preparation and imaging

A.1. TEM sample preparation

It is essential in TEM imaging that the sample preparation procedure creates as little damage to the sample ultrastructure as possible. The standard technique for preparing biological TEM samples containing HA is by ultramicrotomy, i.e., sectioning ultrathin (10–90 nm) sections with a diamond knife and collecting them in a water trough. An advantage of ultramicrotomy over ion milling is the relative ease by which samples can be sectioned; hence it is the only feasible technique for preparing multiple samples. In addition, ultramicrotomy presumably does not lead to the possible phase transformations or altered chemistry that methods such as ion milling might. Concerns have arisen, however, about whether the ultramicrotomy process produces artifacts in the structure of the sections [43]. Previous studies investigating dissolution of HA in the water trough of the ultramicrotome confirmed that there is minimum alteration to the mineral during the ultramicrotomy process [42,44]. An additional concern with ultramicrotomy is that the HA is damaged as a result of impact by the diamond knife [45]. For this reason, TEM samples were additionally prepared in the absence of any mechanical force using a focused-ion beam system. Comparison of sections produced via both techniques showed that there is minimal alteration to the organization of the intertubular mineral. In comparison, the tubule filling was more evident in the FIB-ed sections as intratubular crystallites were seen more extensively attached to the surface of the intertubular dentin in samples prepared by the FIB. These observations validate ultramicrotomy as a sample preparation technique.

A.2. EW reconstruction

In order to analyze the atomic structure of the intratubular dentin, Ångström resolution EW phase images were obtained through focal series reconstruction (Fig. 8). To the authors' knowledge, this is one of the first applications of this technique to characterize the atomic structure of biological materials. A concern with performing focal series reconstructions on such samples is that the time that the sample is exposed to the electron beam is relatively long ($\sim$2 min) which may affect the

ultrastructure. Degradation by the investigating electron beam is a commonly encountered difficulty when imaging apatites in the TEM. The principal effects in imaging decomposition as evidenced by production of voids or bubbles (likely of oxygen) are gradual amorphization of the crystalline lattice, and loss of constituents, notably oxygen, from the thin-foil surface [46]. An earlier high-resolution TEM experiment by Brès et al. [35] described the growth of nano-crystals on the surface of enamel crystals and suggested that these arose as a result of electron-induced beam damage. Our timed-set of beam damage experiments imply that the single crystal mineral grains observed are indeed real and are not formed during electron-beam exposure. No evidence of phase transformation or diffusion-induced crystal growth were observed during exposure to the electron-beam. Hence, we conclude that EW reconstructions can be used to gain atomic resolution on biological structures so long as care is taken with beam exposure and imaging time.

References

[1] Marshall Jr. GW, Marshall SJ, Kinney JH, Balooch M. The dentin substrate: structure and properties related to bonding. J Dent 1997;25:441–58.

[2] Vasiliadis L, Darling AI, Levers BG. The amount and distribution of sclerotic human root dentine. Arch Oral Biol 1983;28: 645–9.

[3] Micheletti CM. Dental histology: study of aging processes in root dentine. Boll Soc Ital Biol Sper 1998;74:19–28.

[4] Vasiliadis L, Darling AI, Levers BG. The histology of sclerotic human root dentine. Arch Oral Biol 1983;28:693–700.

[5] Natusch I, Pilz ME, Klimm W, Buchmann G. Transparent dentinal sclerosis and its clinical significance. Zahn Mund Kieferheilkd Zentralbl 1989;77:3–7.

[6] Giachetti L, Ercolani E, Bambi C, Landi D. Sclerotic dentin: Aetio-pathogenetic hypotheses. Minerva Stomatol 2002;51: 285–92.

[7] van Huysen G. The microstructure of normal and sclerosed dentine. J Prosthetic Dent 1960;10:976.

[8] Kinney JH, Nalla RK, Pople JA, Breunig T, Ritchie RO. Transparent root dentin: mineral concentration, crystallite size, and mechanical properties. Biomaterials 2005;26:3363–76.

[9] Gerould CH. Ultramicrostructure of human tooth as revealed by the electron microscope. J Dent Res 1944;23:239–45.

[10] Shroff FR, Williamson KI, Bertaud WS. Electron microscope study of dentine: the true nature of the dentinal canals. J Oral Surg (Chicago) 1954;7:662–7.

[11] Scott DB. The electron microscopy of enamel and dentine. Ann NY Acad Sci 1955;60:575–85.

[12] Frank RM. Electron microscopy of undecalcied sections of human adult dentine. Arch Oral Biol 1959;1:29–32.

[13] Kerebel B. Dentinogenesis imperfecta: a structural and ultrastructural study. SSO Schweiz Monatsschr Zahnheilkd 1975; 85:1264–81.

[14] Voegel JC, Frank RM. Ultrastructural study of apatite crystal dissolution in human dentine and bone. J Biol Buccale 1977;5: 181–94.

[15] Kerebel B, Daculsi G, Menanteau J, Kerebel LM. The inorganic phase in dentinogenesis imperfecta. J Dent Res 1981;60:1655–60.

[16] Schroeder L, Frank RM. High-resolution transmission electron microscopy of adult human peritubular dentine. Cell Tissue Res 1985;242:449–51.

[17] Frank RM. Structural events in the caries process in enamel, cementum, and dentin. J Dent Res 1990;69:559–66.

[18] Van Meerbeek B, Inokoshi S, Braem M, Lambrechts P, Vanherle G. Morphological aspects of the resin–dentin interdiffusion zone with different dentin adhesive systems. J Dent Res 1992;71: 1530–40.

[19] Inokoshi S, Hosoda H, Harnirattisai C, Shimada Y. Interfacial structure between dentin and seven dentin bonding systems revealed using argon ion beam etching. Oper Dent 1993;18:8–16.

[20] Inokoshi S, Willems G, Van Meerbeek B, Lambrechts P, Braem M, Vanherle G. Dual-cure luting composites. Part i: filler particle distribution. J Oral Rehabil 1993;20:133–46.

[21] Van Meerbeek B, Conn LJJ, Duke ES, Schraub D, Ghafghaichi F. Demonstration of a focused ion-beam cross-sectioning technique for ultrastructural examination of resin-dentin interfaces. Dent Mater 1995;11:87–92.

[22] Houlle P, Voegel JC, Schultz P, Steuer P, Cuisinier FJ. High resolution electron microscopy: structure and growth mechanisms of human dentin crystals. J Dent Res 1997;76:895–904.

[23] Frank RM. Ultrastructure of human dentine 40 years ago—progress and perspectives. Arch Oral Biol 1999;44:979–84.

[24] Kwong S-M, Tay FR, Yip H-K, Kei L-H, Pashley DH. An ultrastructural study of the application of dentine adhesives to acid-conditioned sclerotic dentine. J Dent 2000;28:515–28.

[25] Hashimoto M, Ohno H, Sano H, Kaga M, Oguchi H. In vitro degradation of resin—dentin bonds analyzed by microtensile bond test, scanning and transmission electron microscopy. Biomaterials 2003;24:3795–803.

[26] Yoshida E, Hashimoto M, Hori M, Kaga M, Sano H, Oguchi H. Deproteinizing effects on resin—tooth bond structures. J Biomed Mater Res 2004;68B:29–35.

[27] Daculsi G, LeGeros RZ, Jean A, Kerebel B. Possible physico-chemical processes in human dentin caries. J Dent Res 1987; 66:1356–9.

[28] White JM, Goodis HE, Marshall SJ, Marshall GW. Sterilization of teeth by gamma radiation. J Dent Res 1994;73:1560–7.

[29] Porter AE, Patel N, Skepper JN, Best SM, Bonfield W. Comparison of in vivo dissolution processes in hydroxyapatite and silicon-substituted hydroxyapatite bioceramics. Biomaterials 2003;24:4609–20.

[30] Thust A, Coene WMJ, Op de Beeck M, Van Dyck D. Focal-series reconstruction in HRTEM: Simulation studies on non-periodic objects. Ultramicroscopy 1996;64:211–30.

[31] Thust A, Overwijk MHF, Coene WMJ, Lentzen M. Numerical correction of lens aberrations in phase-retrieval HRTEM. Ultramicroscopy 1996;64:249–64.

[32] O'Keefe MA, Hetherington CJD, Wang YC, Nelson EC, Turner JH, Kisielowski C, Malm J- O, Muller R, Ringnalda J, Pan M, Thust A. Sub angstrom high-resolution transmission electron microscopy at 300 Kv. Ultramicroscopy 2001;89:215–41.

[33] Kisielowski C, Hetherington CJD, Wang YC, Kilaas R, O'Keefe MA, Thust A. Imaging columns of the light elements C, N, and O with sub-angstrom resolution. Ultramicroscopy 2001;89:243–63.

[34] Coene WMJ, Thust A, Op de Beeck M, Van Dyck D. Maximum-likelihood method for focus-variation image reconstruction in high resolution transmission electron microscopy. Ultramicroscopy 1996;64:109–35.

[35] Bres EF, Hutchinson JL, Senger B, Voegel JC, Frank RM. HREM study of irradiation damage in human dental enamel crystals. Ultramicroscopy 1991;35:305–22.

[36] Ziv V, Weiner S. Bone crystal sizes: a comparison of transmission electron microscopic and X-ray diffraction line width broadening techniques. Connect Tissue Res 1994;30:165–75.

[37] Nalla RK, Kinney JH, Ritchie RO. On the fracture of human dentin: Is it stress- or strain-controlled? J Biomed Mater Res 2003;67A:484–95.
[38] Kruzic JJ, Nalla RK, Kinney JH, Ritchie RO. Crack blunting, crack bridging and resistance-curve fracture mechanics in dentin: effect of hydration. Biomaterials 2003;24:5209–21.
[39] Nalla RK, Kruzic JJ, Ritchie RO. On the origin of the toughness of mineralized tissue: microcracking or crack bridging? Bone 2004;34:790–8.
[40] Garnier P, Voegel JC, Frank RM. Dissolution kinetics of synthetic hydroxyapatite and human enamel crystals. J Biol Buccale 1976;4:323–30.
[41] Dean HT, Arnold FA, Elvolve E. Domestic water and dental caries: additonal studies of the relation of fluoride in domestic waters to dental caries in 4425 white children, age 12–14 years of 13 cities in 4 states. Public Health Rep 1942;57:1155–79.
[42] Porter AE, Best SM, Bonfield W. Ultrastructural comparison of hydroxyapatite and silicon-substituted hydroxyapatite for biomedical applications. J Biomed Mater Res 2004;68A:133–41.
[43] Landis WJ, Paine MC, Glimcher MJ. Electron microscopic observations of bone tissue prepared anhydrously in organic solvents. J Ultrastruct Res 1977;59:1–30.
[44] Porter AE, Patel N, Skepper JN, Best SM, Bonfield W. Effect of sintered silicate-substituted hydroxyapatite on remodelling processes at the bone-implant interface. Biomater 2003;25: 3303–14.
[45] Porter AE, Patel N, Skepper JN, Best SM, Bonfield W. Comparison of in vivo dissolution processes in hydroxyapatite and silicon-substituted hydroxyapatite bioceramics. Biomaterials 2003;24:4609–20.
[46] Glaeser RM, Hobbs LW. Radiation damage in stained catalase at low temperature. J Microsc 1975;103:209–14.